Chapter 7

A scaling relation for disk galaxies: circular-velocity gradient *versus* central surface brightness

— **Federico Lelli, Filippo Fraternali, and Marc Verheijen** —

Monthly Notices of the Royal Astronomical Society: Letters, 2013,
doi:10.109/mnrasl/slt053

Abstract

For disk galaxies, a close relation exists between the distribution of light and the shape of the rotation curve. We quantify this relation by measuring the inner circular-velocity gradient $d_R V(0)$ for spiral and irregular galaxies with high-quality rotation curves. We find that $d_R V(0)$ correlates with the central surface brightness μ_0 over more than two orders of magnitude in $d_R V(0)$ and four orders of magnitudes in μ_0. This is a scaling relation for disk galaxies. It shows that the central stellar density of a galaxy closely relates to the inner shape of the potential well, also for low-luminosity and low-surface-brightness galaxies that are expected to be dominated by dark matter.

7.1 Introduction

Scaling relations are an ideal tool to investigate the structure, the formation, and the evolution of galaxies. For disk galaxies, the Tully-Fisher (TF) relation (Tully & Fisher 1977) is one of the best-studied scaling laws. It was originally proposed as a correlation between the absolute magnitude of a galaxy and the width of its global H I line profile. It is now clear that the fundamental relation is between the total baryonic mass of the galaxy and the circular velocity along the flat part of the outer rotation curve ($V_{\rm flat}$), thought to be set by the dark matter (DM) halo (e.g. McGaugh et al. 2000; Verheijen 2001; Noordermeer & Verheijen 2007).

While $V_{\rm flat}$ is related to the total dynamical mass of a galaxy, the inner shape of the rotation curve provides information on the steepness of the potential well. For disk galaxies (Sb and later types), the rotation curve is generally described by an inner rising part (nearly solid-body) and an outer flat part (e.g. Bosma 1981; Begeman 1987; Swaters et al. 2009). For bulge-dominated galaxies, instead, the rotation curve shows a very fast rise in the center, often followed by a decline and the flattening in the outer parts (e.g. Casertano & van Gorkom 1991; Noordermeer et al. 2007).

The relation between the optical properties of a galaxy and the shape of its rotation curve has been debated for many years (e.g. Rubin et al. 1985; Corradi & Capaccioli 1990; Persic & Salucci 1991). Several authors pointed out that the shape of the luminosity profile and the shape of the rotation curve are closely related (Kent 1987; Casertano & van Gorkom 1991; Broeils 1992; Sancisi 2004; Swaters et al. 2009). In particular, de Blok & McGaugh (1996) and Tully & Verheijen (1997) compared the properties of two *disk* galaxies on the same position of the TF relation but with different central surface brightness, and found that high-surface-brightness (HSB) galaxies have steeply-rising rotation curves compared to low-surface-brightness (LSB) ones. Thus, for a given total luminosity (or $V_{\rm flat}$), an exponential light distribution with a shorter scale-length corresponds to a steeper potential well (see also Amorisco & Bertin 2010). For HSB spirals, maximum-disk solutions can explain the dynamics in the central regions with reasonable values of the stellar mass-to-light ratio M_*/L (e.g. van Albada & Sancisi 1986; Palunas & Williams 2000), suggesting that either baryons dominate the gravitational potential or DM closely follows the distribution of light. Garrido et al. (2005) also found a clear trend between the inner slope of the rotation curve and the central surface brightness of 18 HSB spiral galaxies. For LSB galaxies, maximum-disk solutions can reproduce the inner parts of the rotation curves, but they often require high values of M_*/L that cannot be explained by stellar population models (e.g. de Blok et al. 2001; Swaters et al. 2011), leading to the interpretation that LSB galaxies are dominated by DM at all radii. Finally, galaxies with a central "light excess" with respect to the exponential disk (e.g. a bulge) show a corresponding "velocity excess" in the inner parts of the rotation curve (e.g. Márquez & Moles

1999; Swaters et al. 2009). This is usually referred to as the "Renzo's rule" (Sancisi 2004): for any feature in the luminosity profile of a galaxy there is a corresponding feature in the rotation curve, and vice versa.

In this Letter, we show that the inner circular-velocity gradient $d_R V(0)$ of a galaxy strongly correlates with the central surface brightness μ_0 over more than two orders of magnitude in $d_R V(0)$ and four orders of magnitude in μ_0, thereby extending and firmly establishing the correlation hinted at by Fig. 8 of Garrido et al. (2005). This is a scaling relation for disk galaxies. We discuss the implications of this relation for the stellar and DM properties of galaxies.

7.2 Data Analysis

7.2.1 The circular-velocity gradient

We define the circular-velocity gradient $d_R V(0)$ as the inner slope of a galaxy rotation curve, i.e. dV/dR for $R \to 0$. $d_R V(0)$ can be estimated if the rising part of the rotation curve is well sampled, but this requires high-quality data and a careful modelling of the gas kinematics in the inner parts. To minimize the uncertainties, we use four samples of galaxies with high-quality rotation curves: Swaters et al. (2009, hereafter S09), de Blok et al. (2008, hereafter dB08 or THINGS), Verheijen & Sancisi (2001, hereafter VS01), and Begeman (1987, hereafter B87). The rotation curves were derived using interferometric H I observations and corrected for beam-smearing effects. We select only galaxies viewed at inclination angles i between 40° and 80°, as the rotation velocities of face-on disks require a large correction for i, while the observed rotation curves of edge-on disks may be affected by unseen holes in the central H I distribution. We projected each derived rotation curve on to the corresponding position-velocity diagram to verify that they have been properly determined. We exclude the galaxies from S09 and VS01 with low-quality data ($q > 2$; see S09). The spiral NGC 3521 (from dB08) is close to edge-on in the inner regions and we neglect the two innermost velocity points. Five galaxies are in common between B87 and dB08. We use the new rotation curves from THINGS except for two galaxies (NGC 2903 and NGC 3198), as the inner parts of their rotation curves are better traced by B87, who applied a careful beam-smearing correction (see Figs. 9 and 12 of dB08). The sample of S09 has one object (NGC 2366) in common with dB08 and another one (UGC 6446) in common with VS01; we use the rotation curves from S09. In all these cases the differences in $d_R V(0)$ are, however, within a factor of 2. The final sample comprises 63 galaxies with morphological types ranging from Sab to Sd/Im.

To this high-quality sample, we add 11 rotation curves of S0/Sa galaxies (with $40° \leq i \leq 80°$) from Noordermeer et al. (2007, hereafter N07). Since early-type galaxies usually lack H I emission in their central regions, the rotation curves were derived combining Hα long-slit spectroscopy (for the inner parts)

with H I observations (for the outer parts). We exclude UGC 12043 as the Hα observations of this galaxy have very low velocity resolution. The values of $d_R V(0)$ for early-type galaxies are more uncertain than those for late-type galaxies.

We derive $d_R V(0)$ by fitting the inner rotation curve with a polynomial function of the form

$$V(R) = \sum_{\rm n=1}^{m} a_{\rm n} \times R^n \tag{7.1}$$

and consider the linear term $a_1 = \lim_{R\to 0} dV/dR = d_{\rm R}V(0)$. The fit is error-weighted and constrained to pass through $V = 0$ at $R = 0$. The value of a_1 depends on i) the radial range used in the fit, and ii) the order of the polynomial m. We define R_{90} as the radius where the rotation curve reaches 90% of its maximum velocity, and fit only the points within R_{90}. This choice allows us to maximize the number of points along the rising part of the rotation curve without including points along the flat part. Rotation curves with less than 3 points within R_{90} are excluded, as they are not well-resolved in the inner parts. 16 galaxies from the high-quality sample and 3 galaxies from N07 are excluded by this criterion, thus the high-quality and total samples reduce to 47 and 55 objects, respectively. For a pure exponential disk with scale-length $R_{\rm d}$, $R_{90} \simeq 1.2R_{\rm d}$. Thus, the first fitted point of the rotation curve is typically at $R \lesssim 0.4R_{\rm d}$ and the derived value of $d_{\rm R}V(0)$ is representative of the innermost galaxy regions that are accessible by the available rotation curves. To derive the best-fitting order of the polynomial, we proceed as follows. We start with a linear fit ($m = 1$) and progressively increase m until the reduced χ^2 (χ^2_ν) approaches 1. In practice, we minimize the function $P_\chi(\chi^2;\nu) - 0.5$, where $P_\chi(\chi^2;\nu)$ is the integral probability of χ^2 and ν is the number of degrees of freedom; the procedure is halted in case χ^2_ν would drop below 1. Visual inspection showed that this method works better than the F-test (e.g. Bevington & Robinson 2003), that in some cases returns high values of m and thus increases the number of free parameters in the fit.

We test our automatic procedure on a set of model rotation curves, calculated by summing the contributions of a disk, a bulge, and a DM halo. We add typical errors to the velocity points ($\sim$5 km s^{-1}) and try several spatial samplings. We find that, even if the rotation curve is poorly sampled ($\sim$5 points within R_{90}), the actual value of $d_{\rm R}V(0)$ can be recovered with a error of $\sim$30%. However, if the rotation curve has an inner "bump" (due to a compact bulge), $d_{\rm R}V(0)$ may be under estimated by a factor of $\sim$2.

Fig. 7.1 shows the results for four representative galaxies that require polynomial fits of different orders. Late-type galaxies (Sb to Im) are generally well fitted by polynomials with $m = 1$ (e.g. UGC 7559) or $m = 2$ (e.g. NGC 3198), but several cases do require $m \geq 3$ (e.g. NGC 5055). Early-type galaxies (S0/Sa) often require high-order polynomials ($m \geq 4$, e.g. UGC 11670),

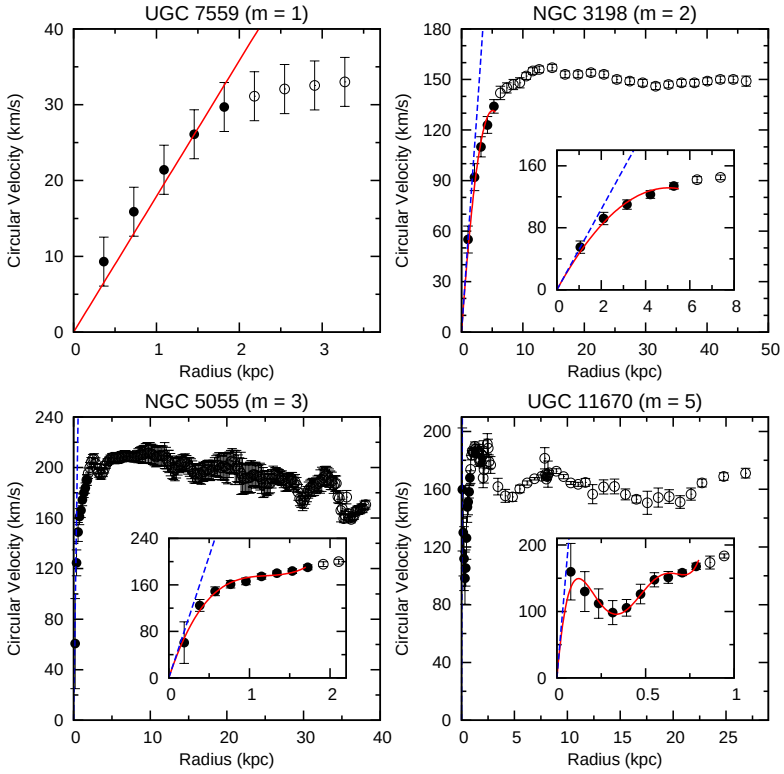

Figure 7.1 – Results of the polynomial fit for four representative galaxies. The filled circles show the points of the rotation curve within R_{90}, while the open circles show the points excluded in the fit. The solid, red line shows the fitted polynomial function, while the dashed, blue line shows its linear term. The order m of the polynomial is indicated. See Sect. 7.2.1 for details.

as their rotation curves may have complex shapes characterized by a steeply-rising part followed by a decline and a second rise. For some bulge-dominated galaxies from N07, the value of $d_R V(0)$ is rather uncertain, since there may be no data points in the inner radial range where the linear term a_1 is representative of the rotation curve (see Fig. 7.1, bottom-right). Table 7.1 provides the fit results for all the galaxies in our sample.

The error $\delta_{d_{\rm R}V(0)}$ on $d_R V(0)$ is estimated as

$$\delta_{d_{\rm R}V(0)} = \sqrt{\delta_{a_1}^2 + \left(d_{\rm R}V(0)\frac{\delta_i}{\tan(i)}\right)^2 + \left(d_{\rm R}V(0)\frac{\delta_{\rm D}}{D}\right)^2} \qquad (7.2)$$

where δ_{a_1} is the nominal error on the fitted linear term a_1, δ_i is the error on the disk inclination i, and $\delta_{\rm D}$ is the error on the galaxy distance D. $\delta_{\rm D}$ typically

gives a negligible contribution for galaxies with distances derived using the tip of the red giant branch (TRGB) and/or Cepheids (Ceph), whereas it can dominate the error budget for galaxies with distances estimated from the TF relation or the Hubble flow.

7.2.2 The central surface brightness

For the high-quality sample of disk-dominated galaxies, we consider two ways to estimate the central surface brightness: i) the disk central surface brightness $\mu_{\rm d}$, obtained from an exponential fit to the outer parts of the luminosity profile, and ii) the observed central surface brightness μ_0, obtained from a linear extrapolation of the luminosity profile in the inner few arcseconds to $R = 0$ (see Swaters & Balcells 2002). μ_0 takes into account possible deviations from a pure exponential disk. This may carry valuable information on the mass distribution, e.g. if a pseudo-bulge/bar is present, but may also reflect variations in the stellar populations and/or in the internal extinction, e.g. if the star-formation activity is enhanced in the central parts. We use the observed central surface brightness μ_0. Since we are considering disk-dominated galaxies (Sb and later types), we correct μ_0 for inclination; we assume an optically-thin disk. Given the ambiguity in using either μ_0 or $\mu_{\rm d}$, we include the difference $\Delta\mu = \mu_{\rm d} - \mu_0$ in the error δ_{μ_0}. This is estimated as

$$\delta_{\mu_0} = \sqrt{(\Delta\mu/2)^2 + [2.5\log(e)\tan(i)\delta_i]^2}. \quad (7.3)$$

For the galaxies from S09, we use the values listed in Table A.5 of Swaters & Balcells (2002) (Harris R-band). For the galaxies from VS01, we use the surface photometry from Tully et al. (1996) (Cousins R-band). For the galaxies from dB08 and B87, we use the surface photometry from three different sources (in order of preference): Swaters & Balcells (2002) (Harris R-band), Kent (1987) (r-band), and Muñoz-Mateos et al. (2009) (Harris R-band or r'-band). The optical filters are comparable, but there can be systematic differences of $\sim$0.1 mag (within the typical errors). Two galaxies from dB08 (NGC 925 and NGC 7793) and one galaxy from B87 (NGC 5371) have no R-band photometry available and have been excluded, reducing the total sample to 52 objects.

The S0/Sa galaxies from N07 require a different approach, because i) the surface brightness rapidly increases in the central regions due to the presence of a dominant bulge; and ii) several galaxies are at large distances ($\gtrsim$30 Mpc), thus the linear resolution of the optical observations is not very high ($\gtrsim$150 kpc). For these galaxies, Noordermeer & van der Hulst (2007) provide the R-band disk central surface brightness $\mu_{\rm d}$, extrapolated from an exponential fit and corrected for i, and the bulge central surface brightness $\mu_{\rm b}$, extrapolated from a Sersic fit to the inner parts after subtracting the disk contribution. We estimate μ_0 by summing the contributions of $\mu_{\rm d}$ and $\mu_{\rm b}$; the latter value is *not* corrected for i as the bulge is assumed to be spherical. The errors are given by Eq. 7.3, where $\Delta\mu$ is now the difference between μ_0 and the innermost value of μ observed.

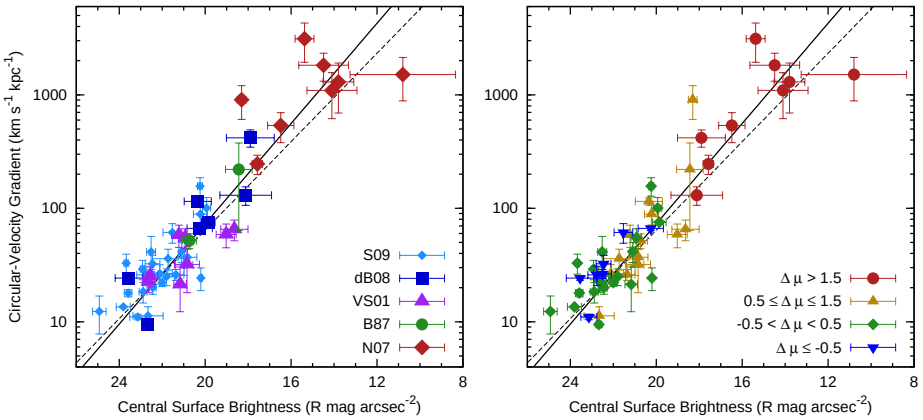

Figure 7.2 – The circular-velocity gradient versus the central surface brightness. The solid and dashed lines show a liner fit to the data points for the total and high-quality samples, respectively. *Left:* galaxies coded by the reference for the rotation curve (S09: Swaters et al. 2009, dB08: de Blok et al. 2008, VS01: Verheijen & Sancisi 2001, B87: Begeman 1987, N07: Noordermeer et al. 2007). *Right:* galaxies coded by the value of $\Delta\mu = \mu_{\rm d} - \mu_0$ (in R mag arcsec^{-2}), that quantifies the "light excess" over an exponential profile.

7.3 The $d_R V(0) - \mu_0$ scaling relation

In Fig. 7.2 (left), we plot μ_0 against $d_R V(0)$ for the total sample of 52 galaxies. There is a clear, striking relation. A linear, error-weighted fit to the data yields

$$\log[d_R V(0)] = (-0.22 \pm 0.02)\,\mu_0 + (6.28 \pm 0.40). \qquad (7.4)$$

As discussed in Sect. 7.2, the values of $d_R V(0)$ for the S0/Sa galaxies from N07 are uncertain. However, it is clear that these bulge-dominated galaxies follow the same trend defined by disk-dominated ones. Fig. 7.2 (left) also shows a linear fit excluding the objects from N07 (dashed line). This gives only slightly different values of the slope (-0.19 ± 0.03) and the intersect (5.70 ± 0.57). Considering the different types of galaxies and the uncertainties involved, the relation shown in Fig. 7.2 is remarkably tight and extended, spanning more than two orders of magnitude in $d_R V(0)$ and four orders of magnitude in μ_0.

The values of the slope and the intersect are likely more uncertain than the formal errors, due to several effects in the determination of $d_R V(0)$ and μ_0. Possible concerns are i) the different linear resolutions (in kpc) of the H I and optical observations, and ii) the effects on μ_0 of internal extinction, recent star-formation, and/or a LINER core. We performed several fits using different methods to estimate μ_0 and $d_R V(0)$, such as calculating V/R at the innermost point of the rotation curve. We obtained slopes always between -0.25 and -0.15, and we think that the actual slope must be constrained between these values.

The scatter around the relation is largely due to observational uncertainties on $d_R V(0)$. Major sources of uncertainties are i) the galaxy distance, ii) the inclination, and iii) the innermost points of the rotation curve (see Eq. 7.2). However, part of the scatter is likely to be intrinsic, partially due to differences in the 3-dimensional (3D) distribution of baryons and in the structural component that defines μ_0 (a disk, a bulge, a bar, or a nuclear star cluster).

To investigate the role played by different structural components, in Fig. 7.2 (right) we plot the same data points coding the galaxies by the value of $\Delta\mu = \mu_{\rm d} - \mu_0$. This quantifies the deviation from an exponential law in the inner parts of the luminosity profile (in R mag arcsec^{-2}). We distinguish between four cases: i) galaxies dominated by a bulge ($\Delta\mu > 1.5$), ii) galaxies with a small central concentration of light ($0.5 \leq \Delta\mu \leq 1.5$) like a pseudo-bulge or a bar, iii) galaxies with an exponential disk ($-0.5 < \Delta\mu < 0.5$), and iv) galaxies with a central light depression ($\Delta\mu \leq -0.5$). The upper-right end of the relation ($\mu_0 \gtrsim 18$ mag arcsec^{-2}) is populated by bulge-dominated galaxies. It is clear that, for these galaxies, the use of $\mu_{\rm d}$ instead of μ_0 would shift them away from the relation, as $\mu_{\rm d} \lesssim$ 19-20 R mag arcsec^{-2} (the "Freeman value", Freeman 1970). On the lower-left end of the relation, instead, one can find both pure exponential disks and galaxies with central light concentrations/depressions. For these disk-dominated galaxies, the use of $\mu_{\rm d}$ instead of μ_0 would still lead to a correlation, but this would have a steeper slope ($\sim$-0.25). For galaxies with similar values of μ_0, $d_R V(0)$ do not seem to depend on the detailed shape of the luminosity profile (simple exponential or with a central light depression/concentration).

7.4 Discussion

The correlation between the central surface brightness μ_0 and the circular-velocity gradient $d_R V(0)$ implies that there is a close link between the stellar density and the gravitational potential in the central parts of galaxies. This holds for both HSB and LSB objects, covering a wide range of masses and asymptotic velocities ($20 \lesssim V_{\rm flat} \lesssim 300$ km s^{-1}).

The relation between the distribution of light and the distribution of mass has been extensively discussed in the past (see Sancisi 2004 and references therein). However, only few attempts have been made to parametrize this relation, notably by S09. Fig. 10 of S09 plots the logarithmic slope between 1 and 2 disk scale-lengths $S_{1,2} = \log[V(2h)/V(h)]/\log(2)$ versus the "light excess" with respect to an exponential disk $\Delta\mu = \mu_{\rm d} - \mu_0$. It shows that a "light excess" (a bulge-like component) corresponds to a "velocity excess" in the rotation curve with respect to the expectations for the underlying exponential disk. The limitation of that parametrization is that it does not capture the dynamical difference between HSB and LSB disks, that are known to have steeply-rising and slowly-rising rotation curves, respectively (e.g. Tully & Verheijen 1997). In Fig. 10 of S09, indeed, both HSB and LSB exponential disks have $\Delta\mu \simeq 0$

and $S_{1,2} \simeq 0.5$. The latter result is due to the fact that $S_{1,2}$ is, by definition, a scale-invariant quantity, that is not expected to depend on μ_0 or $V_{\rm max}$. In contrast, $d_R V(0)$ measures the inner slope of the rotation curve in physical units (km s^{-1} kpc^{-1}) and is directly related to the central dynamical surface density (in $M_\odot$ pc^{-2}), providing insights in the underlying physics, as we now discuss.

For a 3D distribution of mass, the rotation velocity V of a test particle at radius R is given, to a first approximation, by

$$\frac{V^2}{R} = \alpha \frac{G M_{\rm dyn}}{R^2} \tag{7.5}$$

where G is Newton's constant, $M_{\rm dyn} = 4/3\pi R^3 \overline{\rho}_{\rm dyn}$ is the dynamical mass within R, and α is a factor that depends on the detailed mass distribution (for a spherical distribution of mass α=1, while for a thin exponential disk $\alpha \simeq 0.76$ at $R = 0.5 R_0$). For $R \rightarrow 0$, we have

$$\frac{dV}{dR} = \frac{V}{R} = \sqrt{\beta G \rho_{\rm dyn,0}} = \sqrt{\beta G \frac{\rho_{\rm bar,0}}{f_{\rm bar,0}}} \tag{7.6}$$

where $\beta = 4/3\pi\alpha$, $\rho_{\rm dyn,0}$ and $\rho_{\rm bar,0}$ are, respectively, the central dynamical and baryonic mass densities, and $f_{\rm bar,0} = \rho_{\rm bar,0}/\rho_{\rm dyn,0}$ is the baryon fraction in the central regions. Note that $f_{\rm bar,0}$ may strongly differ from the "cosmic" baryon fraction, and can vary widely from galaxy to galaxy, depending on the formation and evolution history. Observationally, we measure μ_0 which is related to $\rho_{\rm bar,0}$ by

$$\mu_0 = -2.5 \log[\rho_{\rm bar,0}\, \Delta z\, (M_{\rm bar}/L)^{-1}] \tag{7.7}$$

where Δz is the typical thickness of the stellar component (either a disk or a bulge) and $M_{\rm bar}/L$ is the baryonic mass-to-light ratio, including molecules and other *dark* baryonic components. Thus, we expect the following relation

$$\log[d_R V(0)] = -0.2\, \mu_0 + 0.5 \log\left(\beta G \frac{M_{\rm bar}/L}{\Delta z\, f_{\rm bar,0}}\right). \tag{7.8}$$

In Sect. 7.3, we mentioned that the slope of our relation is not well-determined due to several uncertainties in the measurements of $d_R V(0)$ and μ_0. However, it is consistent with -0.2 and can be constrained between -0.15 and -0.25. In case the slope would be exactly -0.2, the second term of Eq. 7.8 would be a constant, implying a puzzling fine-tuning between the 3D distribution of baryons (β and Δz), the baryonic mass-to-light ratio ($M_{\rm bar}/L$), and the DM content ($f_{\rm bar,0}$).

Despite the uncertain value of the slope, the results presented here show a clear relation between the central stellar density in a galaxy and the steepness of the potential well (see also Sancisi 2004; Swaters et al. 2011). This implies a

close link between the density of the baryons, regulated by gas accretion, star-formation, and feedback mechanisms, and the central density of the DM halo, together shaping the inner potential well. This may represent a challenge for models of galaxy formation and evolution. Future observational studies may help to better constrain the slope of the relation, while theoretical work should aim to understand its origin.

7.5 Conclusions

We measured the circular-velocity gradient $d_R V(0)$ for a sample of spiral and irregular galaxies with high-quality rotation curves. We found a linear relation between $\log[d_{\rm R} V(0)]$ and the central surface brightness μ_0 with a slope of about -0.2. This is a scaling-relation for disk galaxies that holds for objects of very different morphologies, luminosities, and sizes, ranging from dwarf irregulars to bulge-dominated spirals. This relation quantifies the coupling between visible and dynamical mass in the central parts of galaxies, and shows that the central stellar density closely relates to the inner shape of the potential well.

Acknowledgements

We are grateful to Renzo Sancisi for stimulating discussions and insights. We also thank Erwin de Blok and Rob Swaters for providing us with the high-quality rotation curves. FF aknowledges financial support from PRIN MIUR 2010-2011, project “The Chemical and Dynamical Evolution of the Milky Way and Local Group Galaxies”, prot. 2010LY5N2T.

Table 7.1 – Galaxy sample. The galaxies are listed according to the reference for the rotation curve. The last column provides references for the distance and the surface photometry: a) Tully (1988); b) Tully et al. (2009); c) Tolstoy et al. (1995); d) Hoessel et al. (1998); e) Jacobs et al. (2009); f) Thim et al. (2004); g) Karachentsev et al. (2003); h) Saha et al. (2006); i) Tully et al. (1996); j) Nasa/Ipac Extragalactic Database (NED); k) Willick et al. (1997); l) Swaters & Balcells (2002); m) Kent (1987); n) Muñoz-Mateos et al. (2009); o) Bottema (1989); Noordermeer & van der Hulst (2007).

Name	Type	Dist (Mpc)	Method	i (°)	$\mu_{0,R}$ (mag/$''^2$)	$V_{\rm max}$ (km/s)	$d_R V(0)$ (km/s/kpc)	R_{90} (kpc)	m	χ^2_ν	Ref.
(1)	(2)	(3)	(4)	(5)	(6)	(7)	(8)	(9)	(10)	(11)	(12)
Galaxies from Swaters et al. (2009)											
UGC 731	Im	11.8±4.3	TF	57±3	22.5±0.2	74±3	41±15	5.1	3	0.42	a, l
UGC 2455	IBm	6.4±1.2	TF	51±3	20.2±0.1	61±4	24±5	3.3	2	1.23	a, l
UGC 3371	Im	21.9±4.0	TF	49±3	22.9±0.2	86±3	18±4	11.1	3	0.90	b, l
UGC 3711	IBm	8.2±1.5	TF	60±3	19.6±0.8	95±3	...	0.6	...	...	b, l
UGC 3851	IBm	3.4±0.3	Ceph	59±3	22.5±0.2	55±3	22±2	2.4	1	0.63	c, l
UGC 3966	Im	7.4±1.4	TF	41±3	23.4±0.4	50±4	...	1.1	...	...	a, l
UGC 4173	Im	16.7±3.1	TF	40±3	22.7±0.7	57±4	11±2	8.5	2	0.24	a, l
UGC 4305	Im	3.0±0.2	Ceph	40±3	22.5±0.4	37±3	26±2	1.1	1	0.04	d, l
UGC 4325	Sm?	10.0±1.8	TF	41±3	21.5±0.1	93±3	...	1.4	...	...	a, l
UGC 4499	SBdm	12.8±2.4	TF	50±3	21.0±0.4	74±3	32±6	3.7	2	0.01	a, l
UGC 4543	Sdm	30.0±5.5	TF	46±3	20.6±0.7	67±4	...	2.2	...	...	a, l
UGC 5272	Im	6.5±1.2	TF	59±3	22.8±0.4	45±3	26±5	1.4	1	0.42	a, l
UGC 5414	IBm	9.4±1.7	TF	55±3	22.4±0.3	61±2	32±6	2.7	2	0.06	a, l
UGC 5721	SBd?	5.9±1.1	TF	61±3	19.9±0.2	79±3	101±24	1.3	2	2.70	a, l
UGC 5918	Im	7.1±1.3	TF	46±3	23.7±0.1	44±4	33±6	2.6	2	0.20	a, l
UGC 6446	Sd	18.0±3.0	TF	52±3	20.8±0.4	80±2	37±6	6.5	3	0.20	b, l
UGC 7047	Im	4.3±0.1	TRGB	46±3	22.0±0.1	38±4	22±2	1.6	1	0.51	e, l
UGC 7232	Im pec	2.8±0.5	TF	59±3	21.5±0.4	44±3	61±12	0.6	1	1.02	a, l
UGC 7323	SBdm	5.8±1.0	TF	47±3	21.1±0.1	86±4	42±8	2.9	2	1.38	b, l
UGC 7399	SBdm	8.0±1.5	TF	55±3	20.2±0.3	109±2	89±17	4.6	3	1.11	a, l
UGC 7524	Sm	4.3±0.4	Ceph	46±3	21.4±0.4	84±4	26±3	6.2	2	1.17	f, l
UGC 7559	IBm	5.0±0.2	TRGB	61±3	23.6±0.2	33±3	18±1	1.8	1	0.66	e, l

Table 7.1 – continued.

Name	Type	Dist (Mpc)	Method	i (°)	$\mu_{0,R}$ (mag/$''^2$)	$V_{\rm max}$ (km/s)	$d_R V(0)$ (km/s/kpc)	R_{90} (kpc)	m	χ^2_ν	Ref.
(1)	(2)	(3)	(4)	(5)	(6)	(7)	(8)	(9)	(10)	(11)	(12)
UGC 7577	Im	2.6±0.1	TRGB	63±3	23.1±0.4	18±3	11±1	1.5	1	0.09	e, l
UGC 7603	SBd?	10.5±1.7	TF	78±3	21.8±0.4	64±3	25±4	3.8	2	0.29	b, l
UGC 7690	Im	7.5±1.4	TF	41±3	20.3±0.1	61±4	...	0.5	...	...	a, l
UGC 7866	IBm	4.6±0.2	TRGB	44±3	22.4±0.1	33±4	20±2	1.7	1	1.64	e, l
UGC 7916	Im	7.2±2.6	TF	74±3	24.9±0.3	36±3	12±4	2.6	1	0.96	a, l
UGC 7971	Sm	8.0±1.5	TF	38±3	21.4±0.1	45±4	...	1.7	...	...	a, l
UGC 8490	Sm	4.6±0.6	TRGB	50±3	20.2±0.1	80±4	157±29	1.3	3	0.77	g, l
UGC 8837	IBm	7.2±0.1	TRGB	80±3	23.8±0.3	48±3	13±1	3.1	1	0.02	e, l
UGC 9211	Im	14.7±2.7	TF	44±3	22.9±0.1	66±4	29±6	3.2	2	0.06	a, l
UGC 11707	Sdm	15.7±3.0	TF	68±3	21.7±0.7	100±3	36±7	8.0	3	0.36	a, l
UGC 12060	IBm	15.1±2.8	TF	40±3	21.4±0.2	75±4	...	2.2	...	...	a, l
UGC 12632	Sm	9.2±1.7	TF	46±3	22.1±0.6	76±3	27±5	6.0	2	0.70	a, l
Galaxies from de Blok et al. (2008)											
DDO 154	IBm	4.0±0.1	TRGB	66±3	23.5±0.6	50±5	24±1	4.0	2	1.79	e, l
IC 2574	SBm	3.9±0.1	TRGB	53±3	22.7±0.1	78±5	9±1	8.0	1	0.70	e, l
NGC 925	SBd	9.3±0.2	Ceph	66±3	...	120±6	19±1	9.7	2	0.26	h, -
NGC 2403	SBcd	3.1±0.2	Ceph	63±3	20.3±0.6	144±4	115±8	10.2	5	1.12	h, m
NGC 2841	Sb	14.1±0.4	Ceph	74±3	18.1±1.1	324±4	...	3.8	...	...	h, m
NGC 2976	Sc pec	3.6±0.1	TRGB	64±3	20.2±0.6	86±3	67±3	2.1	2	1.27	e, l
NGC 3031	Sab	3.6±0.3	Ceph	59±3	16.4±1.3	260±7	...	2.4	...	...	h, m
NGC 3521	SBbc	11.2±1.8	TF	73±3	18.1±1.2	233±4	130±24	2.6	2	0.64	b, n
NGC 3621	Sd	7.2±0.2	Ceph	65±3	19.8±0.3	159±3	75±3	18.8	5	0.71	h, n
NGC 3627	SBb	12.6±0.5	Ceph	62±3	17.8±1.0	207±11	...	2.7	...	...	h, n
NGC 4736	Sab	4.7±0.1	TRGB	41±3	16.1±1.2	198±5	...	0.4	...	...	e, n
NGC 4826	Sab	4.7±0.1	TRGB	65±3	18.2±0.6	189±27	...	0.2	...	...	e, n
NGC 5055	Sbc	7.9±1.3	TF	59±3	17.9±1.1	212±8	418±72	1.7	3	0.57	b, n

Table 7.1 – continued.

Name	Type	Dist (Mpc)	Method	i (°)	$\mu_{0,R}$ (mag/$''^2$)	$V_{\rm max}$ (km/s)	$d_RV(0)$ (km/s/kpc)	R_{90} (kpc)	m	χ^2_ν	Ref.
(1)	(2)	(3)	(4)	(5)	(6)	(7)	(8)	(9)	(10)	(11)	(12)
NGC 7331	Sb	15.1±0.7	Ceph	76±3	17.7±1.4	268±13	...	3.1	...	...	h, n
NGC 7793	Sd	3.6±0.1	TRGB	50±3	...	118±4	152±9	3.1	4	0.57	e, -
Galaxies from Verheijen & Sancisi (2001)											
NGC 3877	Sc	15.5±3.0	Cluster	76±1	18.6±0.6	171±5	65±13	3.8	2	0.59	i, i
NGC 3917	Scd	15.5±3.0	Cluster	79±2	21.2±0.3	138±5	21±9	5.3	4	0.58	i, i
NGC 3953	SBbc	15.5±3.0	Cluster	62±1	17.0±0.1	234±8	...	4.5	...	...	i, i
NGC 3972	Sbc	15.5±3.0	Cluster	77±1	20.9±0.2	134±5	55±11	4.5	2	0.60	i, i
NGC 4100	Sbc	15.5±3.0	Cluster	73±2	19.0±0.5	195±6	59±14	3.8	2	0.76	i, i
UGC 6399	Sm	15.5±3.0	Cluster	75±2	22.6±0.3	88±5	23±5	3.8	1	2.67	i, i
UGC 6917	SBd	15.5±3.0	Cluster	56±2	21.2±0.3	111±6	58±13	4.5	3	0.86	i, i
UGC 6983	SBcd	15.5±3.0	Cluster	49±1	20.8±0.6	113±4	32±14	5.3	4	0.71	i, i
UGC 7089	Sdm	15.5±3.0	Cluster	80±3	22.5±0.3	79±7	25±5	5.3	2	0.48	i, i
Galaxies from Begeman (1987)											
NGC 2903	SBbc	8.5±1.4	TF	60±3	18.4±0.6	216±3	220±156	2.5	5	2.67	b, m
NGC 3198	SBc	14.5±2.0	Ceph	71±3	20.7±0.3	157±2	52±8	5.3	2	0.88	h, m
NGC 5033	Sc	18.8±3.0	TF	66±1	18.5±0.7	225±8	...	0.9	...	...	b, m
NGC 5371	SBbc	37.8±7.0	TF	53±2	...	242±3	278±65	6.9	4	5.26	a, -
NGC 6503	Scd	5.3±0.6	TRGB	74±2	19.4±0.4	121±2	...	1.3	...	...	g, o
Galaxies from Noordermeer et al. (2007)											
UGC 2916	Sab	63.4±4.4	Vflow	42±3	16.5±0.6	232±4	538±159	1.1	2	1.33	j, p
UGC 2953	Sab pec	21.6±4.0	TF	50±3	14.5±1.2	334±9	1825±505	5.6	10	5.70	b, p
UGC 3205	Sab	48.9±14.7	Vflow	67±3	18.3±0.2	247±4	905±298	3.5	7	0.20	j, p
UGC 3546	SBa	28.4±5.2	TF	55±3	17.2±0.6	267±12	...	0.6	...	...	a, p
UGC 3580	Sa pec	25.1±4.4	TF	63±3	17.6±0.2	131±2	246±48	18.2	10	3.25	b, p
UGC 6786	S0	29.4±10.8	TF	68±3	10.8±2.4	230±6	1510±626	3.9	7	0.55	a, p
UGC 6787	Sab	21.9±4.0	TF	69±3	13.8±0.7	278±12	1298±607	0.4	2	2.54	a, p

Table 7.1 – continued.

Name	Type	Dist (Mpc)	Method	i (°)	$\mu_{0,R}$ (mag/$''^2$)	$V_{\rm max}$ (km/s)	$d_R V(0)$ (km/s/kpc)	R_{90} (kpc)	m	χ^2_ν	Ref.
(1)	(2)	(3)	(4)	(5)	(6)	(7)	(8)	(9)	(10)	(11)	(12)
UGC 8699	SBab	39.4±6.7	TF	73±3	14.1±1.2	205±2	1093±476	0.9	3	2.12	b, p
UGC 9133	Sab	50.5±8.8	TF	53±3	14.3±0.1	312±6	...	0.3	...	...	k, p
UGC 11670	S0/a	14.2±5.2	TF	70±3	15.4±0.4	191±7	3117±1180	0.8	5	0.33	a, p
UGC 11852	SBa?	81.4±14.2	TF	50±3	16.2±0.6	234±10	...	0.4	...	...	k, p

References

Amorisco, N. C. & Bertin, G. 2010, A&A, 519, A47
Begeman, K. 1987, PhD thesis, University of Groningen
Bevington, P. R. & Robinson, D. K. 2003, Data reduction and error analysis for the physical sciences
Bosma, A. 1981, AJ, 86, 1825
Bottema, R. 1989, A&A, 221, 236
Broeils, A. H. 1992, PhD thesis, University of Groningen
Casertano, S. & van Gorkom, J. H. 1991, AJ, 101, 1231
Corradi, R. L. M. & Capaccioli, M. 1990, A&A, 237, 36
de Blok, W. J. G. & McGaugh, S. S. 1996, ApJL, 469, L89
de Blok, W. J. G., McGaugh, S. S., & Rubin, V. C. 2001, AJ, 122, 2396
de Blok, W. J. G., Walter, F., Brinks, E., et al. 2008, AJ, 136, 2648
Freeman, K. C. 1970, ApJ, 160, 811
Garrido, O., Marcelin, M., Amram, P., et al. 2005, MNRAS, 362, 127
Hoessel, J. G., Saha, A., & Danielson, G. E. 1998, AJ, 115, 573
Jacobs, B. A., Rizzi, L., Tully, R. B., et al. 2009, AJ, 138, 332
Karachentsev, I. D., Sharina, M. E., Dolphin, A. E., et al. 2003, A&A, 398, 467
Kent, S. M. 1987, AJ, 93, 816
Márquez, I. & Moles, M. 1999, A&A, 344, 421
McGaugh, S. S., Schombert, J. M., Bothun, G. D., & de Blok, W. J. G. 2000, ApJL, 533, L99
Muñoz-Mateos, J. C., Gil de Paz, A., Zamorano, J., et al. 2009, ApJ, 703, 1569
Noordermeer, E. & van der Hulst, J. M. 2007, MNRAS, 376, 1480
Noordermeer, E., van der Hulst, J. M., Sancisi, R., Swaters, R. S., & van Albada, T. S. 2007, MNRAS, 376, 1513
Noordermeer, E. & Verheijen, M. A. W. 2007, MNRAS, 381, 1463
Palunas, P. & Williams, T. B. 2000, AJ, 120, 2884
Persic, M. & Salucci, P. 1991, ApJ, 368, 60
Rubin, V. C., Burstein, D., Ford, Jr., W. K., & Thonnard, N. 1985, ApJ, 289, 81
Saha, A., Thim, F., Tammann, G. A., Reindl, B., & Sandage, A. 2006, ApJS, 165, 108
Sancisi, R. 2004, in IAU Symposium, Vol. 220, Dark Matter in Galaxies, ed. S. Ryder, D. Pisano, M. Walker, & K. Freeman, 233
Swaters, R. A. & Balcells, M. 2002, A&A, 390, 863
Swaters, R. A., Sancisi, R., van Albada, T. S., & van der Hulst, J. M. 2009, A&A, 493, 871
Swaters, R. A., Sancisi, R., van Albada, T. S., & van der Hulst, J. M. 2011, ApJ, 729, 118
Thim, F., Hoessel, J. G., Saha, A., et al. 2004, AJ, 127, 2322
Tolstoy, E., Saha, A., Hoessel, J. G., & McQuade, K. 1995, AJ, 110, 1640
Tully, R. B. 1988, Nearby galaxies catalog

Tully, R. B. & Fisher, J. R. 1977, A&A, 54, 661
Tully, R. B., Rizzi, L., Shaya, E. J., et al. 2009, AJ, 138, 323
Tully, R. B. & Verheijen, M. A. W. 1997, ApJ, 484, 145
Tully, R. B., Verheijen, M. A. W., Pierce, M. J., Huang, J.-S., & Wainscoat, R. J. 1996, AJ, 112, 2471
van Albada, T. S. & Sancisi, R. 1986, Royal Society of London Philosophical Transactions Series A, 320, 447
Verheijen, M. A. W. 2001, ApJ, 563, 694
Verheijen, M. A. W. & Sancisi, R. 2001, A&A, 370, 765
Willick, J. A., Courteau, S., Faber, S. M., et al. 1997, ApJS, 109, 333